Korean J. Chem. Eng., 35(7), 1423-1432 (2018)
DOI: 10.1007/s11814-018-0046-4

pISSN: 0256-1115
eISSN: 1975-7220

Linear and non-linear analyses on the onset of miscible viscous fingering in a porous medium

Won Sun Ryoo* and Min Chan Kim,†**

*Department of Chemical Engineering, Hongik University, Seoul 04066, Korea
**Department of Chemical Engineering, Jeju National University, Jeju 63243, Korea
(*Received 31 January 2018 • accepted 12 March 2018*)

Abstract−The onset of miscible viscous fingering in porous media was analyzed theoretically. The linear stability equations were derived in the self-similar domain, and solved through the modal and non-modal analyses. In the non-modal analysis, adjoint equations were derived using the Lagrangian multiplier technique. Through the non-modal analysis, we show that initially the system is unconditionally stable even in the unfavorable viscosity distribution, and there exists the most unstable initial disturbance. To relate the theoretical predictions with the experimental work, non-linear direct numerical simulations were also conducted. The present stability condition explains the system more reasonably than the previous results based on the conventional quasi-steady state approximation.

Keywords: Viscous Fingering, Non-modal Analysis, Modal Analysis, Linear Stability Analysis, Direct Numerical Simulation

INTRODUCTION

Miscible viscous fingering which deforms parallel viscosity contours into fingerlike patterns occurs in porous media when a less viscous fluid displaces another miscible, more viscous fluid, i.e., viscosity increases along the direction of propagation [1]. This interesting phenomenon plays an important role in many engineering fields, such as enhanced oil recovery, pollution spreading in soils, chromatographic column design, and so on [2-7]. Also, viscous fingering is important to understand how gastric mucin protects gastric epithelium from strong HCl in mammalian stomachs [8,9]. To analyze the onset and evolution of viscous fingering many researchers have studied experimentally and theoretically.

By using X-ray imaging, Slobod and Thomas [2] and Perkins et al. [3] determined the onset and the evolution of the miscible fingering experimentally. They showed that in the high flow rate run fingers are present and absent near the injection region in the low flow rate run. Their experimental results mean that there is a stable region even if the viscosity distribution is unfavorable. Its stability characteristics are influenced by the viscosity distribution and, also, the flow rate. Further evidence of fingering has been reported by using nuclear magnetic resonance (NMR) imaging technique [10], optical method [11], and echo-planar spectroscopic imaging method [12]. First theoretical analysis was conducted by Tan and Homsy [4], based on the quasi-steady state approximation (QSSA). They suggested that the unfavorable viscosity distribution makes the system unconditionally unstable and induces viscous fingering instability. Their QSSA has been used as a standard method to analyze the related problems [13-16]. Although the validity of QSSA can be guaranteed for the region of $\tau(=R^2U_0X/D)>>1$, here R is the log-viscosity ratio, U_0 is the uniform injection velocity, D is the isotropic dispersion coefficient and X is the streamwise distance, many researchers [13-17] applied the QSSA even for $\tau\rightarrow 0$, i.e., they conducted the initial growth rate analyses under the QSSA. To compensate the QSSA results, Tan and Homsy [4,18] conducted transient analyses by solving the same problem using initial value (IV) problem methods, where they introduced random noise as an initial condition and monitored its growth. They showed that the disturbances under the unfavorable viscosity distribution have a large negative growth rate during the early stage of displacing.

Although the above-mentioned theoretical analyses gave some insights into the onset of viscous fingering in the miscible system qualitatively, direct quantitative comparison between the experiments and theoretical analyses has not been tried. Also, the following fundamental questions still remain in connection with the onset of fingering motion: (1) what kind of initial disturbance, if any, occurs? (2) where can the instability motion be observed experimentally?

To answer the above questions, we analyzed the onset condition of viscous fingering using linear stability analysis and nonlinear numerical simulation. To find the most practical initial condition, we derived new linear stability equations in the self-similar domain. By applying non-modal analysis based on the Lagrangian multiplier technique (Doumenc et al. [19]) into the present system, we derived additional adjoint equations. By solving the stability equations and their adjoint ones iteratively we identified the most practical initial condition, and traced its temporal evolution. In section 4.2, the present non-modal analysis is compared with the present modal analysis and the generalized stability theory. Based on the initial disturbance identified under the linear stability analysis, we tried to answer the more practical problem, question (2), through non-linear numerical simulations. The previous numerical simulation results [6,18] showed that there exists a position where dispersion length L_d starts to deviate from the theoretically obtained

†To whom correspondence should be addressed.
E-mail: mckim@jejunu.ac.kr

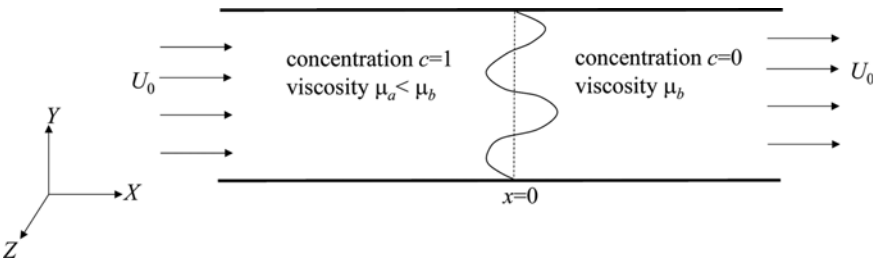

Fig. 1. Schematic diagram of the system considered here.

value. However, in the present study we considered the mass flux, J, across the initial phase boundary, and considered τ_m at which $dJ/d\tau=0$ as an onset position of non-linear viscous fingering. Also, we compared the theoretically obtained τ_m with the previous experimental data.

GOVERNING EQUATIONS AND BASE SYSTEM

If one Newtonian fluid displaces another miscible Newtonian one with the uniform velocity U_0, as schematized in Fig. 1, the governing equations consisting of the Darcy law and mass transport equation in the Lagrangian coordinate system moving at the injection velocity U_0 can be expressed as [4,6]:

$$\nabla\cdot\mathbf{U}=0, \tag{1}$$

$$\nabla P=-\frac{\mu(C)}{K}(\mathbf{i}U_0+U), \tag{2}$$

$$\frac{\partial C}{\partial t}+\mathbf{U}\cdot\nabla C=\nabla\cdot(\mathcal{D}\nabla C), \tag{3}$$

where μ(C) is the concentration dependent viscosity, K is the constant permeability and **i** is the unit vector along the main flow direction, t is the time and $\mathcal{D}$ is the isotropic dispersion coefficient. Here, we assume that fluids are neutrally buoyant and the viscosity-concentration relation has the following form:

$$\mu=\mu_b\exp\left(-R\frac{C-C_b}{C_a-C_b}\right), \tag{4}$$

with the constant log-viscosity ratio R{=ln(μ_b/μ_a)} [4,6,14,16].

In dimensionless form, the above equations can be rewritten as

$$\nabla\cdot\mathbf{u}=0, \tag{5}$$

$$\nabla p=-\overline{\mu}\left(\mathbf{u}+\frac{\mathbf{i}}{R}\right), \tag{6}$$

$$\frac{\partial c}{\partial\tau}+\mathbf{u}\cdot\nabla c=\nabla^2 c, \tag{7}$$

where the velocity, pressure, viscosity and solute concentration are nondimensionalized as $\mathbf{u}=\mathbf{U}/(RU_0)$, $p=K(P-P_0)/(\mu_b\mathcal{D})$, $\overline{\mu}=\mu/\mu_b$ and $c=(C-C_b)/(C_a-C_b)$, respectively. Here $\mathbf{P}_0$ is an arbitrary reference pressure. We use the characteristic length $\mathcal{D}/(RU_0)$ and $\mathcal{D}/(RU_0^2)$ time. The subscripts 'a' and 'b' mean the displacing phase and the displaced phase, respectively. Then, Eq. (4) can be rewritten as

$$\overline{\mu}=\exp(-Rc). \tag{8}$$

We use RU_0 rather than U_0 in the above velocity disturbance, length and time scaling relations, because the instabilities are driven by the velocity, U_0, and the viscosity contrast, R.

The base concentration profile is governed by

$$\frac{\partial c_0}{\partial\tau}=\frac{\partial c_0}{\partial x^2}, \tag{9}$$

under the following initial and boundary conditions:

$$c_0(0, x)=1-H(x), \tag{10a}$$

$$c_0(\tau,\infty)=c_0(\tau,-\infty)-1=0, \tag{10b}$$

where H(x) is the Heaviside unit step function. Using the Laplace transform method, Eqs. (9) and (10) can be solved as

$$c_0(\tau, x)=\frac{1}{2}\mathrm{erfc}\left(\frac{\xi}{2}\right), \tag{11}$$

where $\xi(=x/\sqrt{\tau})$ is the similarity variable and x=0 is the initial interface position.

LINEAR STABILITY ANALYSIS (LSA)

1. Stability Equations

Under linear stability theory, by perturbing Eqs. (5)-(7), the stability equations are derived as

$$\nabla^2 u_1+\frac{1}{\overline{\mu}_0}\frac{\partial\overline{\mu}_0}{\partial x}\frac{\partial u_1}{\partial x}=\frac{1}{R}\frac{1}{\overline{\mu}_0}\nabla_1^2\overline{\mu}_1, \tag{12}$$

$$\frac{\partial c_1}{\partial\tau}+u_1\frac{\partial c_0}{\partial x}=\nabla^2 c_1, \tag{13}$$

where the subscripts '0' and '1' mean the basic and disturbance quantities, respectively. Here, we linearized the viscosity function as

$$\overline{\mu}(c_0+c_1)\approx\overline{\mu}_0+\overline{\mu}_1=\exp(-Rc_0)+\left.\frac{\partial\overline{\mu}}{\partial c}\right|_{c_0}c_1. \tag{14}$$

Using the Fourier mode analysis, the above equations are reduced as

$$\begin{bmatrix}\frac{\partial}{\partial\tau}-\left(\frac{\partial^2}{\partial x^2}-k^2\right) & \frac{\partial c_0}{\partial x}\\ -k^2 & \frac{\partial^2}{\partial x^2}-R\frac{\partial c_0}{\partial x}\frac{\partial}{\partial x}-k^2\end{bmatrix}\begin{bmatrix}c_1\\ u_1\end{bmatrix}=\begin{bmatrix}0\\ 0\end{bmatrix}, \tag{15}$$

where k is the wavenumber showing spanwise periodicity. The proper boundary conditions are

$c_1 \to 0$ and $u_1 \to 0$ as $x \to \pm\infty$. (16)

In the present study, since the base concentration field can be expressed by using the similarity variable ξ, we express the disturbance equations in the (τ, ξ)-domain as

$$\begin{bmatrix} \tau\frac{\partial}{\partial\tau} - (\mathcal{L}_\xi - k^{*2}) & \sqrt{\tau}\frac{\partial c_0}{\partial\xi} \\ -k^{*2} & \frac{\partial^2}{\partial\xi^2} - R\frac{\partial c_0}{\partial\xi}\frac{\partial}{\partial\xi} - k^{*2} \end{bmatrix} \begin{bmatrix} c_1 \\ u_1 \end{bmatrix} = \begin{bmatrix} 0 \\ 0 \end{bmatrix}, \quad (17)$$

under the condition of

$c_1 \to 0$ and $u_1 \to 0$ as $\xi \to \pm\infty$. (18)

where $\mathcal{L}_\xi = \left(\frac{\partial^2}{\partial\xi^2} + \frac{\xi}{2}\frac{\partial}{\partial\xi}\right)$, $k^* = k\sqrt{\tau}$ and $\frac{\partial c_0}{\partial\xi} = -\frac{1}{2\sqrt{\pi}}\exp\left(-\frac{\xi^2}{4}\right)$. Keep in mind that Eqs. (15) and (16) and Eqs. (17) and (18) are mathematically equivalent except for the singular limit $\tau = 0$. Also, some other researchers have used this kind of coordinate transform in similar problems [20-24].

2. Spectral Expansion

In the original (τ, x)-domain, the spectral expansion described in the present section is not possible because the eigenfunctions of the operator d^2/dx^2 cannot meet the boundary conditions (16). Therefore, further analytical approach without the quasi-steady state approximation (QSSA) is not possible in the (τ, x)-domain. Here, by following Kim and Choi's [25-28] approach, the linear stability equations, (17) and (18), were solved by a spectral method in the (τ, ξ)-domain. Using the generalized Fourier series c_1 and u_1 are expressed as

$$c_1(\tau, \xi) = \sum_{n=0}^{\infty} A_n(\tau)\phi_n(\xi), \quad (19)$$

$$u_1(\tau, \xi) = \sum_{n=0}^{\infty} A_n(\tau)\psi_n(\xi). \quad (20)$$

The solutions of $\phi_n(\xi)$ and $\psi_n(\xi)$ are fully discussed in Kim and Choi [25-28]. For the limiting case of R<<1, the stability Eqs. (17) and (18) become parameterless and can be attacked analytically. Note that for this limiting case, Kim [28] expressed $\psi_n(\xi)$ as a recursive relation. This is another reason why we use RU_0 rather than U_0 as a proper velocity scale.

Applying these solutions into Eq. (17) and performing orthogonalization process, we obtain the following equations:

$$\tau\frac{d\mathbf{a}}{d\tau} = \mathbf{E}\mathbf{a}, \quad (21a)$$

$$\mathbf{a} = [A_0, A_1, A_2\cdots]^T, \quad (21b)$$

$$[\mathbf{E}]_{ij} = \int_{-\infty}^{\infty} \exp\left(\frac{\xi^2}{4}\right)\phi_{i-1}(\mathcal{L}_\xi - k^{*2})\phi_{j-1}d\xi - \frac{\sqrt{\tau}}{2\sqrt{\pi}}\int_{-\infty}^{\infty}\phi_{i-1}\psi_{j-1}d\xi. \quad (21c)$$

Kim [28] showed that for the extreme case of R<<1, the matrix $\mathbf{E}$ is symmetric since $\int_{-\infty}^{\infty}\phi_j\psi_i d\xi = \int_{-\infty}^{\infty}\phi_i\psi_j d\xi$.

3. Non-modal Analysis (NMA)

In the non-modal analysis, we should consider all the possible initial conditions, which gives a maximum gain at the optimization position τ_f. Thus, we should find the initial $\mathbf{a}_i$ which gives the maximum gain $G^*(\tau; \tau_i)$ defined as

$$G^*(\tau; \tau_i) = \sqrt{\mathbf{a}^T\mathbf{a}}/\sqrt{\mathbf{a}_i^T\mathbf{a}_i}. \quad (22)$$

Also, based on this quantity, we defined the growth rate as

$$\sigma^* = \frac{1}{G^*}\frac{dG^*}{d\tau}. \quad (23)$$

In the present study, we solved this optimization problem using the Lagrangian multiplier technique suggested by Doumenc et al. [19]. Following their procedure, we formulated the Lagrangian in the (τ, ξ)-domain as

$$\begin{aligned}\mathcal{L} = \|c_1\|_{\tau_f} - s(\|c_1\|_{\tau_i} - 1) - \int_{\tau_i}^{\tau_f}\int_{-\infty}^{\infty}\Big\{&\left(D^2 - R\frac{\partial c_0}{\partial\xi}D - k^{*2}\right)u_1 \\ &- k^{*2}c_1\}\hat{\psi}(\tau, \xi)f_u(\xi)d\xi d\tau - \int_{\tau_i}^{\tau_f}\int_{-\infty}^{\infty}\Big\{\tau\frac{\partial c_1}{\partial\tau} - (\mathcal{L}_\xi - k^{*2})c_1 \\ &+ \frac{\partial c_0}{\partial\xi}\sqrt{\tau}u_1\Big\}\hat{\theta}(\tau, \xi)f_c(\xi)d\xi d\tau\end{aligned} \quad (24)$$

where $\|c_1\| = \int_{-\infty}^{\infty} c_1^2\exp(\xi^2/4)d\xi$ and $D = \partial/\partial\xi$. The second term of the right hand side is the constraint such that $\|c_1\|_{\tau_i} = 1$, s is a scalar Lagrangian multiplier, the adjoint variables $\hat{\psi}$ and $\hat{\theta}$ are the Lagrangian multipliers dependent on τ and ξ. It is known that $f_c(\xi) = \exp(\xi^2/4)$ and $f_u(x) = \exp(-Rc_0)$ are the weight functions of the operators $\mathcal{L}_\xi$ and $\left(D^2 - R\frac{\partial c_0}{\partial\xi}D\right)$, respectively. The above Lagrangian leads to

$$\begin{aligned}\mathcal{L} = \|c_1\|_{\tau_f} - s(\|c_1\|_{\tau_i} - 1) - \int_{\tau_i}^{\tau_f}\int_{-\infty}^{\infty}\Big\{&\left(D^2 - R\frac{1}{2\sqrt{\pi}}\exp\left(-\frac{\xi^2}{4}\right)D - k^{*2}\right)u_1 \\ &- k^{*2}c_1\}\hat{\psi}(\tau, \xi)f_u(\xi)d\xi d\tau - \int_{\tau_i}^{\tau_f}\int_{-\infty}^{\infty}\Big\{\tau\frac{\partial c_1^*}{\partial\tau} - (\mathcal{L}_\xi - k^{*2})c_1 \\ &- \frac{1}{2\sqrt{\pi}}\exp\left(-\frac{\xi^2}{4}\right)\sqrt{\tau}u_1\Big\}\exp\left(\frac{\xi^2}{4}\right)\hat{\theta}(\tau, \xi)d\xi d\tau\end{aligned} \quad (25)$$

In the present study the optimal condition was assumed such that the variation of the Lagrangian is zero: $\delta\mathcal{L} = 0$. This means that

$$\begin{aligned}\delta\mathcal{L} = \int_{-\infty}^{\infty} 2c_1\delta c_1\exp\left(\frac{\xi^2}{4}\right)d\xi - s\left\{\int_{-\infty}^{\infty} 2c_{1,i}\delta c_{1,i}\exp\left(\frac{\xi^2}{4}\right)d\xi\right\} \\ - \int_{\tau_i}^{\tau_f}\int_{-\infty}^{\infty}\hat{\psi}D\{f_u(\xi)D\delta u_1\} - f_u(\xi)\hat{\psi}(k^{*2}\delta u_1 + k^{*2}\delta c_1)d\xi d\tau \\ - \int_{\tau_i}^{\tau_f}\int_{-\infty}^{\infty}\Big\{\tau\frac{\partial\delta c_1}{\partial\tau} - (\mathcal{L}_\xi - k^{*2})\delta c_1 \\ - \frac{1}{2\sqrt{\pi}}\exp\left(-\frac{\xi^2}{4}\right)\sqrt{\tau}\delta u_1\Big\}\exp\left(\frac{\xi^2}{4}\right)\hat{\theta}d\xi d\tau\end{aligned} \quad (26)$$

After performing the integrations by parts, the following relation is obtained:

$$\dot{\delta\mathcal{L}} = \int_{-\infty}^{\infty} 2c_1\delta c_1 \exp\left(\frac{\xi^2}{4}\right)d\xi - s\left\{\int_{-\infty}^{\infty} 2c_{1,i}\delta c_{1,i}\exp\left(\frac{\xi^2}{4}\right)d\xi\right\}$$
$$-\int_{-\infty}^{\infty}\delta c_1\exp\left(\frac{\xi^2}{4}\right)\pi\hat{\theta}\,d\xi\Big|_{\tau_i}^{\tau_f} - \int_{\tau_i}^{\tau_f} f_u(\xi)(D\delta u_1\hat{\psi} - \delta u_1 D\hat{\psi})\Big|_{-\infty}^{\infty} d\tau$$
$$+\int_{\tau_i}^{\tau_f} D\delta c_1\exp\left(\frac{\xi^2}{4}\right)\hat{c} - \delta c_1\exp\left(\frac{\xi^2}{4}\right)D\hat{\theta}\Big|_{-\infty}^{\infty} d\tau - \int_{\tau_i}^{\tau_f}\int_{-\infty}^{\infty}\left\{D(f_u(\xi)D\hat{\psi})\right. \quad (27)$$
$$\left. -k^{*2}f_u(\xi)\hat{\psi} - \frac{\sqrt{\tau}}{2\sqrt{\pi}}\hat{\theta}\right\}\delta u_1\,d\xi\,d\tau - \int_{-\infty}^{\infty}\int_{\tau_f}^{\tau_i}\left\{\hat{\theta} - \tau\frac{\partial\hat{\theta}}{\partial\tau} + (\mathcal{L}_\xi - k^{*2})\hat{\theta}\right.$$
$$\left. +k^{*2}\exp\left(-\frac{\xi^2}{4}\right)f_u(\xi)\hat{\psi}\right\}\delta c_1\exp\left(\frac{\xi^2}{4}\right)d\tau\,d\xi = 0$$

We chose δc_1 and $\hat{\theta}$ which satisfy the boundary conditions for c_1, and δu_1 and $\hat{\psi}$ which satisfy the boundary conditions for u_1. Then the fourth and fifth terms become zero. The optimality conditions are met if $\hat{\psi}$ and $\hat{\theta}$ satisfy the following adjoint problem:

$$\left\{D^2 + \frac{R}{2\sqrt{\pi}}\exp\left(-\frac{\xi^2}{4}\right)D - k^{*2}\right\}\hat{\psi} = \frac{\sqrt{\tau}}{2\sqrt{\pi}}\frac{1}{f_u(\xi)}\hat{\theta}, \quad (28)$$

$$\left(-\hat{\theta} + \tau\frac{\partial\hat{\theta}}{\partial\tau}\right) - (\mathcal{L}_\xi - k^{*2})\hat{\theta} = k^{*2}\exp\left(-\frac{\xi^2}{4}\right)f_u(\xi)\hat{\psi}, \quad (29)$$

$$\int_{-\infty}^{\infty} 2c_1\delta c_1\exp\left(\frac{\xi^2}{4}\right)d\xi - 2\left\{\int_{-\infty}^{\infty} 2c_{1,i}\delta c_{1,i}\exp\left(\frac{\xi^2}{4}\right)d\xi\right\}$$
$$-\int_{0}^{\infty}\delta c_1\exp\left(\frac{\xi^2}{4}\right)\pi\hat{\theta}\,d\xi\Big|_{\tau_i}^{\tau_f} = 0, \quad (30)$$

$$-\int_{\tau_i}^{\tau_f}(D\delta u_1\hat{\psi} - \delta u_1 D\hat{\psi})\Big|_{-\infty}^{\infty} d\tau$$
$$+\int_{\tau_i}^{\tau_f}\exp\left(\frac{\xi^2}{4}\right)(D\delta c_1\hat{\theta} - \delta c_1 D\hat{\theta})\Big|_{-\infty}^{\infty} d\tau = 0. \quad (31)$$

Here, Eq. (29) should be integrated from τ_f to τ_i.

By setting $\hat{\theta} = \pi\hat{c}$ and $\hat{\psi} = \pi\hat{u}$ the adjoint equations reduce to

$$\begin{bmatrix} \tau\frac{\partial}{\partial\tau} - (\mathcal{L}_\xi - k^{*2}) & -k^{*2}\exp\left(-\frac{\xi^2}{4}\right)f_u(\xi) \\ -\frac{1}{f_u(\xi)}\frac{\sqrt{\tau}}{2\sqrt{\pi}} & D^2 + R\frac{1}{2\sqrt{\pi}}\exp\left(-\frac{\xi^2}{4}\right)D - k^{*2} \end{bmatrix}\begin{bmatrix}\hat{c}\\ \hat{u}\end{bmatrix} = \begin{bmatrix}0\\0\end{bmatrix}, \quad (32)$$

under the following boundary conditions:

$$\hat{\psi}\to 0 \text{ and } \hat{c}\to 0 \text{ as } \xi\to\pm\infty. \quad (33)$$

Eq. (30) gives the coupling conditions to connect the stability problem (17) and (18) and its adjoint problem (32) and (33) as

$$2sc_1 = \hat{c} \text{ at } \tau = \tau_i, \quad (34a)$$
$$2c_1 = \hat{c} \text{ at } \tau = \tau_f. \quad (34b)$$

The above Eqs. (32) and (33) are rewritten in the (τ, x)-domain as

$$\begin{bmatrix} \frac{\partial}{\partial\tau} - \left(\frac{d^2}{dx^2} - k^2\right) & k^2\frac{\partial c_0}{\partial x}\exp(-Rc_0) \\ -\exp(Rc_0) & \left(\frac{d^2}{dx^2} - R\frac{\partial c_0}{\partial x} - k^2\right) \end{bmatrix}\begin{bmatrix}\hat{c}\\ \hat{u}\end{bmatrix} = \begin{bmatrix}0\\0\end{bmatrix}, \quad (35)$$

and

$$\hat{u}\to 0 \text{ and } \hat{c}\to 0 \text{ as } x\to\pm\infty. \quad (36)$$

By expressing $\hat{\theta}$ and $\hat{\omega}$ as

$$\hat{c}(\tau, \xi) = \sum_{n=0}^{\infty}\hat{A}_n(\tau)\phi_n(\xi), \quad (37)$$

$$\hat{u}(\tau, \xi) = \sum_{n=0}^{\infty}\hat{A}_n(\tau)\hat{\psi}_n(\xi), \quad (38)$$

we can get the following relations:

$$\left\{D^2 + \frac{R}{2\sqrt{\pi}}\exp\left(-\frac{\xi^2}{4}\right)D - k^{*2}\right\}\hat{\psi}_i = \frac{\sqrt{\tau}}{2\sqrt{\pi}}\frac{1}{f_u(\xi)}\phi_i, \quad (39)$$

under the following boundary conditions

$$\hat{\psi}_n\to 0 \text{ as } \xi\to\pm\infty. \quad (40)$$

Similar to Eq. (25), the solution of the above boundary value problem can be given as

$$\hat{\psi}_i(\xi) = \frac{\sqrt{\tau}}{2\sqrt{\pi}}\int_{-\infty}^{\infty}\hat{G}(\xi, \zeta)\frac{1}{f_u(\zeta)}\phi_i(\zeta)\,d\zeta, \quad (41)$$

where $\hat{G}(\xi, \zeta)$ is the Green's function of the adjoint problem.

Applying these solutions into Eq. (32) and performing orthogonalization process, we obtain

$$\tau\frac{d\hat{\mathbf{a}}}{d\tau} = \hat{\mathbf{E}}\hat{\mathbf{a}}, \quad (42a)$$

$$\hat{\mathbf{a}} = [\hat{A}_0, \hat{A}_1, \hat{A}_2, \cdots]^T, \quad (42b)$$

$$\hat{E}_{ij} = -(\lambda_{i-1} - k^{*2})\delta_{ij} - \frac{\sqrt{\tau}}{2\sqrt{\pi}}k^{*2}$$
$$\int_{-\infty}^{\infty}\int_{-\infty}^{\infty}\phi_{i-1}(\xi)\{f_u(\xi)/f_u(\zeta)\}G(\xi, \zeta)\phi_{j-1}(\zeta)\,d\zeta\,d\xi. \quad (42c)$$

For the limiting case of R<<1, where $f_u(\xi)\to 1$, and therefore $\hat{\mathbf{E}} = \mathbf{E}$, the above adjoint equation becomes

$$\tau\frac{d\hat{\mathbf{a}}}{d\tau} = \mathbf{E}\hat{\mathbf{a}} \text{ for } R<<1. \quad (43)$$

In summary, the present non-modal analysis is to find the most unstable disturbance satisfying Eqs. (21) and (43) under the following coupling conditions:

$$\mathbf{a} = \hat{\mathbf{a}} \text{ at } \tau = \tau_i \text{ and } \tau = \tau_f, \quad (44)$$

which corresponds to Eq. (34). For the limiting case of R<<1, the optimal initial condition is independent of the optimization position τ_f and $\hat{\mathbf{a}} = \mathbf{a}$ should be satisfied because the stability equation and its adjoint are identical. Furthermore, the improvement of the initial condition through the adjoint equation cannot be expected for the limiting case of R<<1. For the finite R, we should depend

on the numerical method, which will be discussed later.

4. Modal Analysis (MA)

In the modal stability analysis, the growth rate is determined by the maximum value of the eigenvalues of **E** in Eq. (21):

$$\sigma^*\tau=\max\{\mathrm{eig}(\mathbf{E})\}. \tag{45}$$

The same results can be obtained from the quasi-steady state approximation (QSSAξ) in the (τ, ξ)-domain [23,24]. Here, we assume that the spatial-temporal dependencies can be separable as:

$$[u_1(\tau,\xi), c_1(\tau,\xi)]=[\bar{u}_1(\xi), \bar{c}_1(\xi)]\exp(\sigma^*\tau), \tag{46}$$

which corresponds to $\frac{\partial c_1}{\partial \tau}=\sigma^* c_1$. Now, the stability equation is reduced to

$$\sigma^*\tau\mathbf{a}=\mathbf{E}\mathbf{a}, \tag{47}$$

and the growth rate can be obtained from $\sigma^*\tau=\max\{\mathrm{eig}(\mathbf{E})\}$. The element of matrix **E** can be obtained by the procedure described in the above section. Because the growth rate from Eq. (47) is identical with Eq. (45), both approaches give same stability characteristics.

As discussed in the above section, for the case of finite R the calculation of the matrix element is not straightforward. So, under the QSSAξ we reduce the stability equations to

$$\begin{bmatrix} \sigma^*\tau-(\mathcal{L}_\xi-k^{*2}) & -\frac{\sqrt{\tau}}{2\sqrt{\pi}}\exp\left(-\frac{\xi^2}{4}\right) \\ k^{*2} & D^2+R\frac{1}{2\sqrt{\pi}}\exp\left(-\frac{\xi^2}{4}\right)D-k^{*2} \end{bmatrix}\begin{bmatrix}\bar{c}_1\\ \bar{u}_1\end{bmatrix}=\begin{bmatrix}0\\0\end{bmatrix}, \tag{48}$$

where $D=d/d\xi$. The proper boundary conditions are

$$\bar{c}_1\to 0 \text{ and } \bar{u}_1\to 0 \text{ as } \xi\to\pm\infty. \tag{49}$$

We solve the above equations with the well-known numerical shooting method [29]. The neutral stability curves obtained by setting $\sigma^*\tau=0$ are compared in Fig. 3. As shown in this figure, third approximation (3-term approximation) is quite enough to explain the stability characteristics.

Farrell and Ioannou [30] suggested a slight modification on the QSSA. According to their idea for the non-autonomous system, the growth rate σ^* can be expressed as

$$\sigma^*\left(=\frac{1}{|\mathbf{a}|}\frac{d|\mathbf{a}|}{d\tau}\right)=\frac{1}{2}\frac{1}{\mathbf{a}^T\mathbf{a}}\left(\frac{d\mathbf{a}^T}{d\tau}\mathbf{a}+\mathbf{a}^T\frac{d\mathbf{a}}{d\tau}\right), \tag{50}$$

since $|\mathbf{a}|=\sqrt{\mathbf{a}^T\mathbf{a}}$. Through the basic matrix operation, the above growth rate is reduced to

$$\sigma^*\tau=\frac{1}{\mathbf{a}^T\mathbf{a}}\mathbf{a}^T\left\{\frac{(\mathbf{E}^T+\mathbf{E})}{2}\right\}\mathbf{a}. \tag{51}$$

All symmetric matrices are normal and all eigenvalues of the normal matrix are all real. Through the eigen analysis it is known that

$$\sigma^*\tau=\max\left\{\mathrm{eig}\left(\frac{\mathbf{E}+\mathbf{E}^T}{2}\right)\right\}, \tag{52}$$

where max{eig(**M**)} represents the maximum eigenvalue of the matrix **M**. For the extreme case of R<<1, since $\mathbf{E}=\mathbf{E}^T$, the growth rate is further reduced to

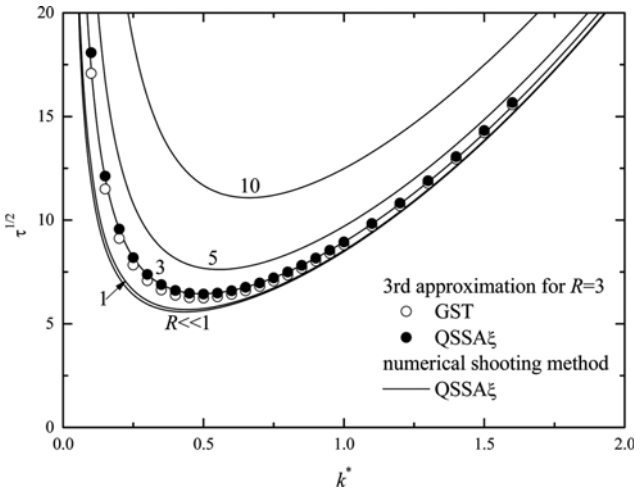

Fig. 2. Neutral stability curves from the various methods.

$$\sigma^*\tau=\max\{\mathrm{eig}(\mathbf{E})\}, \tag{53}$$

which is identical with the result from the QSSAξ, see Eq. (47). In Fig. 2, the neutral stability curve based on the generalized stability theory (GST) is compared with that based on the QSSA for the case of R=3. This figure suggests that the GST yields slightly more unstable disturbance than the QSSAξ in the (τ, ξ)-domain.

NUMERICAL SIMULATIONS

The previous analytical analyses give some information on the onset of miscible viscous fingering. However, the long-term flow behavior such as the growth and amplification of onset disturbances is governed by nonlinear disturbance dynamics. We solve Eqs. (5)-(7) with a numerical method and compare nonlinear numerical simulation results with those from the analytical analyses.

1. Formulation

By taking double curls on Eq. (6) and with the aid of Eq. (5), the velocity field can be reduced to

$$\nabla^2\mathbf{u}=-\nabla\times\omega, \tag{54}$$

$$\omega=-\nabla c\times(\mathbf{u}+\mathbf{i}/R). \tag{55}$$

The convection-dispersion equation can be expressed as

$$\frac{\partial c}{\partial\tau}=\nabla^2 c+j, \tag{56}$$

$$j=-\mathbf{u}\cdot\nabla c. \tag{57}$$

In the 2-dimensional (x, y)-domain, the governing equations for velocity and concentration fields can be reduced to

$$\left(\frac{\partial^2}{\partial x^2}+\frac{\partial^2}{\partial y^2}\right)u=-\frac{\partial\omega_z}{\partial y}, \tag{58a}$$

$$\left(\frac{\partial^2}{\partial x^2}+\frac{\partial^2}{\partial y^2}\right)v=\frac{\partial\omega_z}{\partial x}, \tag{59a}$$

$$\omega_z=\left\{R\left(\frac{\partial c_0}{\partial x}+\frac{\partial c_1}{\partial x}\right)v-\frac{\partial c_1}{\partial y}(u+1)\right\}, \tag{60}$$

$$\frac{\partial c_1}{\partial \tau}=\left(\frac{\partial^2}{\partial x^2}+\frac{\partial^2}{\partial y^2}\right)c_1+j, \tag{61a}$$

$$j=-u\left(\frac{\partial c_0}{\partial x}+\frac{\partial c_1}{\partial x}\right)-v\frac{\partial c_1}{\partial y}. \tag{62}$$

Here, we decompose the concentration field as

$$c(\tau, x, y)=c_0(\tau, x)+c_1(\tau, x, y), \tag{63}$$

and $c_0(\tau, x)$ is already given in Eq. (11).

To solve Eqs. (58)-(62), we employ the Fourier-spectral numerical scheme described in Zimmerman and Homsy [32]. The periodic boundary conditions are taken in both the *x*- and *y*-directions. The use of these boundary conditions has no influence on the dynamics of the concentration front as long as the unstable propagating front does not encounter its periodic extension.

2. Linear Non-modal Analysis

As discussed in section 3.2, fully analytical approach is possible only for R<<1. However, in case of finite R, i.e., non-normal system, we cannot guarantee that the first eigenmode is the most unstable initial disturbance. It is well-known that for a non-normal system, an initial disturbance can grow in time even though all the eigen-modes of the system are damping [33]. Here, for the finite R system, we try to identify the optimal initial condition by solving linearized stability equations and their adjoint ones, numerically. In the linear analysis the vorticity and convective flux defined in Eqs. (60) and (62) are degenerated as

$$\omega_z=\left\{R\frac{\partial c_0}{\partial x}v-\frac{\partial c_1}{\partial y}\right\}, \tag{64a}$$

$$j=-u\frac{\partial c_0}{\partial x}. \tag{65a}$$

Also, from adjoint Eqs. (35) and (36), the adjoint forms of the above quantities can be written as

$$\left(\frac{\partial^2}{\partial x^2}+\frac{\partial^2}{\partial y^2}\right)\hat{u}=-\frac{\partial \hat{\omega}_z}{\partial y}, \tag{58b}$$

$$\left(\frac{\partial^2}{\partial x^2}+\frac{\partial^2}{\partial y^2}\right)\hat{v}=\frac{\partial \hat{\omega}_z}{\partial x}, \tag{59b}$$

$$\frac{\partial \hat{c}_1}{\partial \tau}=\left(\frac{\partial^2}{\partial x^2}+\frac{\partial^2}{\partial y^2}\right)\hat{c}_1+\hat{j}, \tag{61b}$$

$$\hat{\omega}_z=\left\{R\frac{\partial c_0}{\partial x}\hat{v}-\frac{\partial \hat{c}_1}{\partial y}\exp(-Rc_0)\right\}, \tag{64b}$$

$$\hat{j}=-\hat{u}\frac{\partial c_0}{\partial x}\exp(Rc_0). \tag{65b}$$

Note that for the limiting case of R<<1, the above two sets of equations are identical. Here, the magnitude of the disturbance $|c_1|$ is defined as

$$|c_1|=\left[\frac{1}{l_x\cdot l_y}\int_{-l_x/2}^{l_x/2}\int_0^{l_y}c_1^2\,dy\,dx\right]^{1/2}. \tag{66}$$

Based on this quantity, we define its gain $G(\tau;\ \tau_i)$ and growth rate σ as

$$G(\tau;\ \tau_i)=|c_1|_\tau/|c_1|_{\tau_i}, \tag{67}$$

and

$$\sigma=\frac{1}{|c_1|}\frac{d|c_1|}{d\tau}. \tag{68}$$

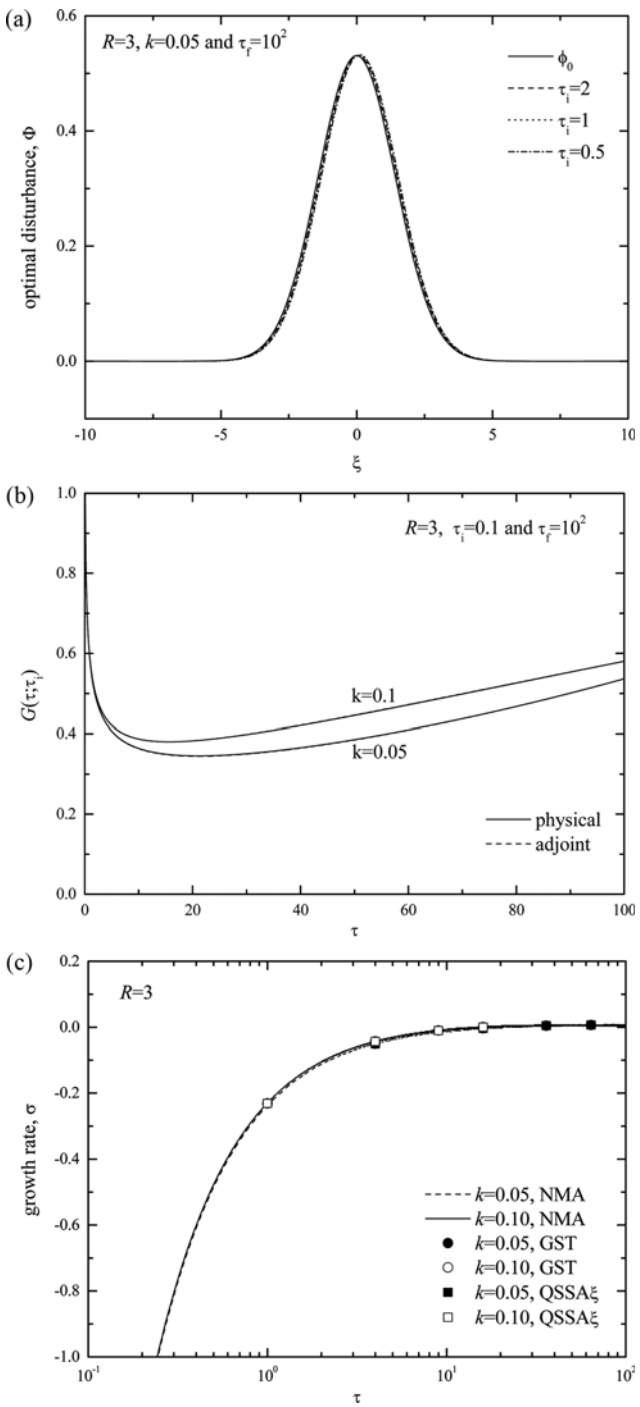

Fig. 3. Results of non-modal analysis: (a) Effect of initiation time on the shape of an optimal initial condition, (b) comparison of the temporal evolution of optimal disturbances in physical and adjoint problems, and (c) comparison of the growth rates from the various methods.

The growth rates σ^* and σ can be related as [24,34]

$$\sigma = \sigma^* + \frac{1}{4\tau} \tag{69}$$

For the limiting case of R<<1, Kim [27] showed that $c_1(\tau, \xi) = A_0(\tau)\phi_0(\xi)$ is the optimal initial condition.

For the finite R system, the present numerical scheme is used to find out the optimal initial disturbance by solving the linear stability equations (58a), (59a), (61a), (63a) and (65a) and their adjoint ones, (58b), (59b), (61b), (64b) and (65b). To determine the optimal initial disturbance giving the maximum amplification of the disturbance, following Doumenc et al's [19] approach, we integrated the stability equations, forward to $\tau = \tau_f$, using the initial guess for c_1 at $\tau = \tau_i$. Then, using the coupling condition, they obtained the final conditions for the adjoint equations. They integrated the adjoint equations backwardly to $\tau = \tau_i$. The newly obtained initial condition for the adjoint equation was used for the improved initial conditions for the stability equations. We used $\Phi = \phi_0(\xi_i)$ as a starting point and continued the above procedure until a predetermined convergence criterion, $\{|c_1|_{\tau_i} - |c_1|_{\tau_i}\}/|c_1|_{\tau_i} < 10^{-3}$ was achieved.

For the case of R=3 and k=0.05, the effect of initiation time on the optimal disturbance is summarized in Fig. 3(a). Fig. 3(b) shows that the optimal disturbance is insensitive to the initiation time, τ_i, the optimization time, τ_f, because the gains obtained from by solving physical and adjoint problems are nearly the same for the whole time range. Also, the optimal disturbance is not affected by the wavenumber of the disturbance k. The growth rates of the present optimal initial condition are compared with the present GST and QSSAξ in Fig. 3(c). This figure shows that the present modal and non-modal analyses give the nearly same growth rate and, therefore, support each other. Furthermore, the optimal disturbance seems not to be influenced by the driving force, R, as shown in Fig. 4.

3. Direct Numerical Simulation (DNS)

In the previous analyses, the wavelength of the disturbances is fixed throughout the simulation. However, the wavelength selection and the nonlinear phenomena such as mixing and mass transfer rate enhancement, the break of symmetry, and the widening of fingering structures are not possible in the linear single-mode analysis. In this section, the calculation domain is set to [0, 2000]×[−1000, 1000], and 2048×2048 collocation points are used. Unlike the linear MA, the initiation condition is important in the nonlinear analysis. Since the linear stability analysis cannot suggest the dominant initial wavenumber in the present simulation, the following initial condition is employed:

$$c_1 = \varepsilon\Phi(\xi_i)\ \text{rand(y)} \text{ at } \tau = \tau_i, \tag{70}$$

where ε means the initial disturbance level, $\Phi(\xi_i)$ is the optimal initial disturbance determined in the previous NMA and rand(y) is the pseudo-random number uniformly distributed between −1 and 1. This condition prevents unphysical conditions of c>1 or c<0, if ε is small enough. For the region of τ~0, the base concentration gradient $\frac{\partial c_0}{\partial x}(\sim -\delta(x))$ shows non-analytic feature and leads to bad convergence properties. For this reason, at all the non-linear numerical simulations the disturbance given in (70) are introduced at τ_i=0.1.

Since we are interested in the enhancement of mixing or mass transfer driven by the instability motion, the mass flux is examined here. The dimensionless vertical mass flux at the initial front x=0, J, which can be written as the sum of contributions from the base diffusion state, J_0, and the convective motion, J_1:

$$J = J_0 + J_1. \tag{72}$$

The diffusional flux can be computed explicitly from the base concentration profile as

$$J_0 = -\left.\frac{\partial c_0}{\partial x}\right|_{z=0} = \frac{1}{\sqrt{4\pi\tau}}. \tag{72}$$

The vertical convective flux is calculated from the horizontal mean of the vertical gradient of c_1 at x=0 as [35]

$$J_1 = \frac{1}{L_y}\int_0^{L_y}\left\{-\left.\frac{\partial c_1}{\partial x}\right|_{x=0}\right\}dy = \frac{1}{L_x L_y}\int_{-L_x/2}^{L_x/2}\int_0^{L_y} u c_1\, dy\, dx. \tag{73}$$

The effect of the random number sequence on the convective

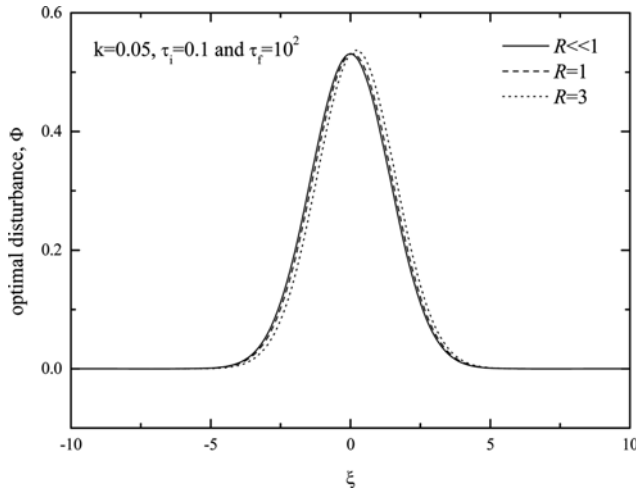

Fig. 4. The effect of R-values on the optimal disturbance.

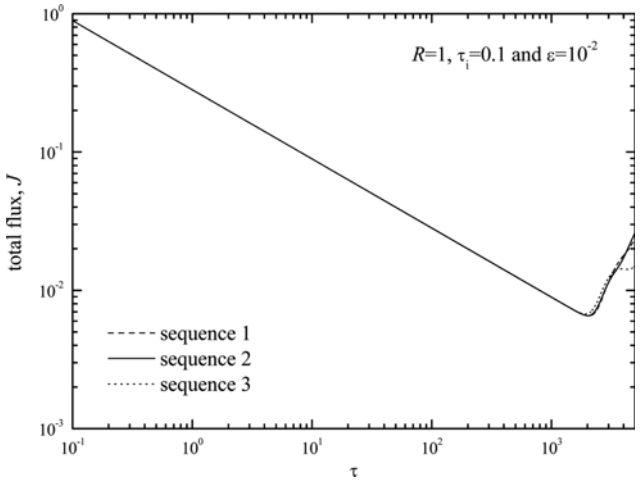

Fig. 5. The effect of the random sequence on the temporal evolution of the total flux for the typical case of R=1, τ_i=0.1 and ε=0.01.

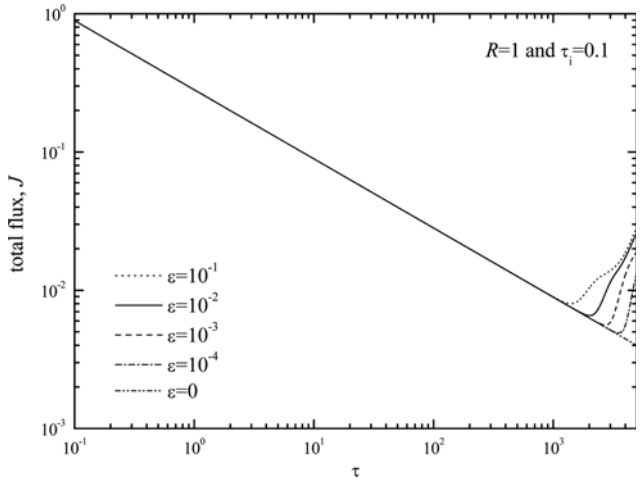

Fig. 6. The effect of the initial disturbance level on the temporal evolution of the total flux for the typical case of R=1 and τ_i=0.1.

flux is summarized in Fig. 5. As shown, the random number sequence has little effect on the convective flux. To consider the effect of the amplitude of the initial disturbance on the total flux J, the convective flux J_1 for three different simulations for R=1 is shown in Fig. 6. Regardless of the magnitude of the initial disturbance, during the initial period diffusion dominates over convection and the disturbances remain in the linear region. From Figs. 5 and 6, we can define two characteristic times τ_c at which $dJ_1/d\tau=0$ and τ_m at which $dJ/d\tau=0$. Note that τ_c from which the convective flux starts to grow is insensitive to the initial condition, whereas τ_m from which the nonlinear terms begin to dominate is strongly dependent on the initial disturbance magnitude. Furthermore, the result for the case of $\varepsilon=0$ follows the diffusion state. This means that the present instability motion is driven by the physical disturbance rather than the numerical errors. However, for a real physical system it is difficult to characterize the amplitude and shape of initial disturbances. From now on, we use Eq. (75) with $\tau_i=0.1$ and $\varepsilon=0.01$ as an initial condition.

RESULTS AND DISCUSSION

Most of the previous studies introduced the quasi-steady state approximation in the (τ, x)-domain (QSSA) or frozen-time model [4-7]. However, as discussed by Ben et al. [21] and Kim and Choi [25], the QSSA in the untransformed (τ, x)-coordinates are not valid at small times, and therefore an analysis in the similarity coordinates (τ, ξ) is required. The present result on the initial growth rate, Eq. (53), and Tan and Homsy's [4] IV calculation results show that the system is stable, $\sigma<0$, in the case of $\tau<1$. According to their IV calculation, initially the system is stable for the random disturbance and even the disturbance from their QSSA at $\tau=0$. Furthermore, the present initial growth rate study explains Slobod and Thomas' [2] experimental result: near the initial displacing front (see their Fig. 1), no fingering is found in the low flow rate experiment and a single bulging finger is observed at the far downstream. Later Perkins et al. [3] reported, in their Table 1, the experimentally determined critical length from which the fingering motion was observed. From these experimental results, there may exist a critical length (or critical time) to develop a fingering instability even for the case of unfavorable viscosity distribution.

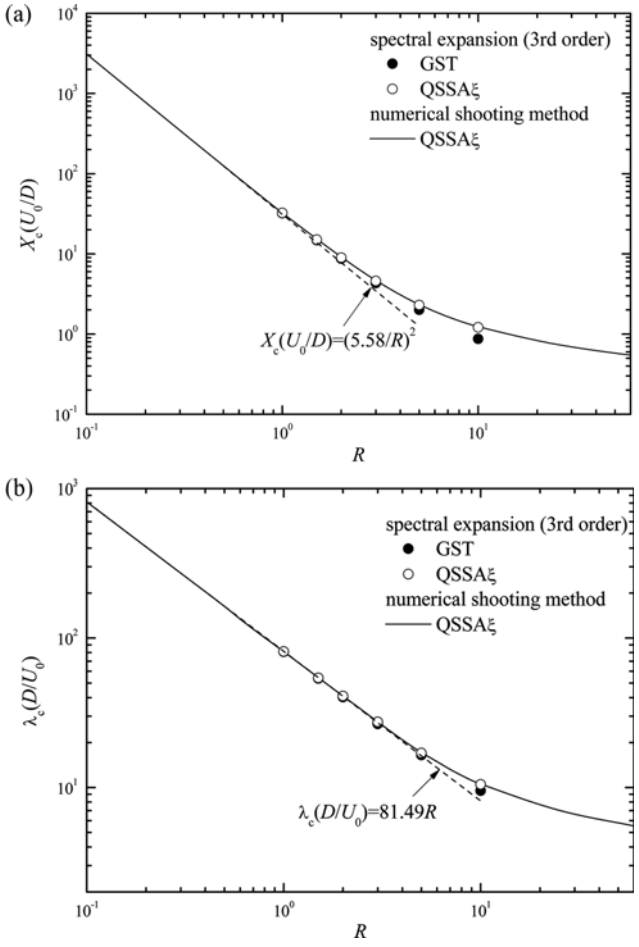

Fig. 7. Comparison of the onset conditions between the GST and QSSAξ: (a) Critical position and (b) critical wave length. The relation of $l_c(D/U_0)$=81.49R is obtained from Eq. (79b).

As discussed in section 3.4, the validity of the QSSAξ depends on the symmetricity of the characteristic matrix **E**. For the limiting cases of R=1, it has been shown that the characteristic matrix **E** is symmetric and therefore, the neutral stability curves using the QSSAξ are the nearly the same as those obtained under GST, as shown in Fig. 3. This figure also shows that the present QSSAξ represents the stability characteristics reasonably well for the system of moderate R. For the case of various R, the critical conditions which can be obtained from the minimum value of neutral stability curve are summarized in Fig. 7. This figure shows that the larger R makes the system more unstable and the critical wavelength larger. It is known that the present QSSAξ works quite well for the system of moderate R and gives good approximation even for the system of large R.

Here, let us focus on the critical conditions to induce the fingering instability. To determine the critical condition the stability criterion is necessary. As discussed in the initial growth rate section, regardless of the value of R, initially σ^* has a negative value. As the

time increases, the convective term, $-\frac{\sqrt{\tau}}{2\sqrt{\tau}}\int_{-\infty}^{\infty}\phi_j\psi_i d\xi$ in Eq. (21c), grows and dominates the dispersion related term, $\int_{-\infty}^{\infty}\exp\left(\frac{\xi^2}{4}\right)\phi_{i-1}$ $(\mathcal{L}_\xi - k^{*2})\phi_{j-1}d\xi$ in Eq. (21c), which makes the system stable. The condition of $\sigma^*=0$ means that two terms are in equilibrium. Based on this, $\sigma^*=0$ is chosen as a neutral stability condition. Based on the results of third approximation, the critical time τ_c and the critical wavenumber at τ_c can be obtained as

$$\tau_c\{=X_cR^2(U/\mathcal{D})\}=5.58^2 \text{ and } \frac{2\pi}{\lambda_c R}(\mathcal{D}/U)\tau_c^{1/2}=0.43, \qquad (79a \& b)$$

where λ_c is the wavelength at the onset time.

Even though linear stability analysis gives important information on the stability of the viscous fingering system, experimental findings such as the enhancement of mass transfer and mixing driven by the instability are strongly dependent on the nonlinear convection. Therefore, the onset of nonlinear convection is of considerably practical importance. Employing the Fourier spectral method, De Wit et al. [6] solved Eqs. (1)-(4) numerically by introducing random initial noise and determined the onset time. They defined the dispersion length L_d as

$$\langle c(\tau, x)\rangle = 0.01 \text{ at } x = L_d, \qquad (80)$$

and monitored temporal evolution of L_d. Here $\langle c(\tau, x)\rangle$ is the laterally averaged concentration. To characterize the nonlinear effect, they defined τ_d as the time when L_d starts to deviate from the curve for R=0. For the range of 0.5<R<4, De Wit et al. [6] suggested the relation τ_d~constant, which is quite similar to the present linear stability result, Eq. (79a). However, they did not try to relate the linear stability analysis with their nonlinear simulation. Here, we have defined the onset time of nonlinear convection, τ_m, as the time at which $dJ/d\tau=0$ and tried to connect this time with the experimentally determined onset condition.

In the present study, to relate the theoretical analyses and the experimental work we conducted the non-linear DNS by solving Eqs. (1)-(4). To start the DNS simulation we introduced the initial condition for Eq. (3). The growth of the instability is strongly dependent on motion of the initial condition. Therefore, the selection of the physically acceptable initial condition is an important problem to relate the DNS and the experiments. Recently, for the gravitational fingering problem Daniel et al. [36] suggested that the initial disturbance localized around the base concentration front is more physical. As shown in Fig. 4, the initial condition determined by the present NMA satisfies Daniel et al's [36] suggestion; however, the initial disturbance given by the QSSA is not localized. If the maximum of $c_0+\varepsilon c_1$ and the minimum of $c_0-\varepsilon c_1$ are considered, the present initial disturbance gives $\max(c_0+\varepsilon c_1)\le 1$ and $\min(c_0-\varepsilon c_1)\ge 0$ if $\varepsilon<0.1$. This means that the unphysical situation of c>1 and c<0 does not appear if a disturbance whose initial magnitude ε less than 0.1 is imposed. However, if the most unstable disturbance identified in Tan and Homsy's [4] QSSA is used as an initial condition, its magnitude should be 0 to avoid the unphysical situation. Since this zero-magnitude initial disturbance of $c_1=0$, cannot induce the instability motion, the following physical constraint impose an important restriction on choosing the initial disturbance:

$$0\le(c_0\pm\varepsilon c_1)\le 1 \text{ for positive small } \varepsilon. \qquad (81)$$

All the physical disturbances should satisfy the above physical constraint.

By introducing the initial fluctuation obtained from the present NMA rather than a random noise as a starting point for the nonlinear calculation, we conducted nonlinear DNS studies. For the various R-values, the total fluxes and convective ones are summarized in Fig. 8. Two characteristic times τ_c and τ_m are shown with the linear stability analysis (LSA) result in Fig. 9. This figure suggests that the growth period is required for the disturbance which sets in at τ_c to increase the mass flux.

The present linear and nonlinear analyses should be checked by

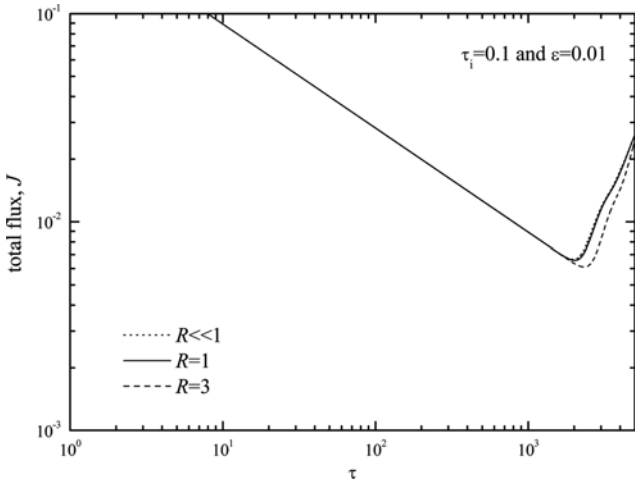

Fig. 8. The effect of the log-viscosity ratio R on the temporal evolution of the total flux for the typical case of τ_i=0.1 and ε=0.01.

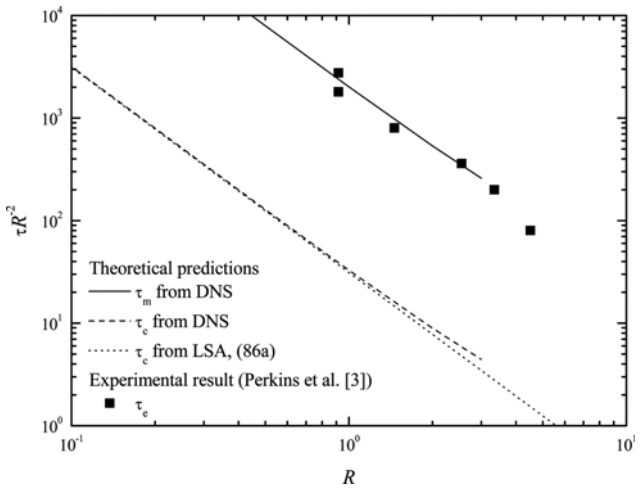

Fig. 9. Comparison of the predicted critical times with the experimental result. For the purpose of comparison, (U_0/D)=400 cm^{-1} is assumed in the Perkins et al.'s [3] experiment.

the systematic experiments. However, as far as we know, the quantitative results were suggested by only Perkins et al. [3]. They measured the average distance X_e at which the fingering is initiated (see their Table 1). From the relation of $\tau=R^2U_0X/\mathcal{D}$, the experimentally determined critical time τ_e can be obtained. However, the dispersion coefficient $\mathcal{D}$ is a complex function of the effective diffusivity D_e, the displacing velocity U_0 and the porous matrix structure. In Perkins et al's [3] experimental data, X_e is independent of U_0 for the large mobility ratio. From this result, $\mathcal{D}\propto U_0$ can be assumed and no further data can be obtained. For the purpose of comparison, $(U_0/\mathcal{D})$=400 cm is assumed in their experiments and their experimental τ_e is compared with the present τ_c in Fig. 9. This figure shows that the present τ_c is too short to explain the experimental results. However, the present τ_m predicts the experimental trend quite well even though τ_m is strongly dependent on the initial magnitude of the disturbance and the value of $(U_0/\mathcal{D})$. This discrepancy is due to the growth period of the disturbances, *i.e.* the amplitude of the disturbance at $\tau=\tau_c$ is too weak to be detected experimentally. Therefore, the growth period for the disturbances to grow is necessary. This difference between the present τ_c based on the linear stability theory and the experimentally determined critical time can be explained by solving the nonlinear Eqs. (1)-(4) directly.

CONCLUSIONS

The onset condition of viscous fingering was analyzed using the linear and non-linear theories. For the linear stability analysis, the stability equations were derived in the similar domain. They were solved analytically and numerically by using non-modal analysis (NMA) and modal analysis (MA). Through the NMA, it is shown that the most feasible optimal initial condition is very similar to the zeroth spectral mode, and initially the present system is unconditionally stable to this optimal initial disturbance. The present NMA and MA yield nearly the same growth rate and explain the previous transient linear and nonlinear ones. Furthermore, the present linear analysis does not violate the physical relevance condition, whereas the previous work based on the conventional quasi-steady state approximation (QSSA) yielded unphysical disturbance, which gives negative concentration. Therefore, the discrepancy between the conventional QSSA and initial value (IV) calculation was resolved in the present analysis. Using the optimal initial disturbance identified in the present NMA, we conducted non-linear direct numerical simulations (DNS). The present DNS study explains the extant experimental results quantitatively. From above findings, it is believed that the present analysis will give a new framework to connect the theoretical predictions with the experimental work.

ACKNOWLEDGEMENT

This research was supported by the Basic Science Research Program through the National Research Foundation of Korea (NRF) funded by the Ministry of Education (NRF-2015R1D1A3A01015798).

REFERENCES

1. S. Hill, *Chem. Eng. Sci.*, **1**, 247 (1952).
2. R. L. Slobod and R. A. Thomas, *Soc. Pet. Eng. J.*, **3**, 9 (1963).
3. T. E. Perkins, O. E. Johnston and R. N. Hoffman, *Soc. Pet. Eng. J.*, **5**, 301 (1965).
4. C. T. Tan and G. M. Homsy, *Phys. Fluids*, **29**, 3549 (1986).
5. G. M. Homsy, *Ann. Rev. Fluid Mech.*, **19**, 271 (1987).
6. A. De Wit, Y. Bertho and M. Martin, *Phys. Fluids*, **17**, 054114 (2005).
7. G. Rousseaux, A. De Wit and M. Martin, *J. Chromatogr. A*, **1149**, 254 (2007).
8. K. R. Bhaskar, P. Garik, B. S. Turner, J. D. Bradley, R. Bansil, H. E. Stanley and J. T. LaMont, *Nature*, **360**, 458 (1982).
9. T. Fujita, S. Ohara, T. Sugaya, K, Saigenji and K. Hotta, *Comp. Biochem. Physiol. B*, **126**, 353 (2000).
10. L. D. Plante, P. M. Romano and E. J. Fernandez, *Chem. Eng. Sci.*, **49**, 2229 (1994).
11. B. S. Broyles, R. A. Shalliker, D. E. Cherrak and G. Guiochon, *J. Chromatogr. A*, **822**, 173 (1998).
12. M. L. Dickson, T. T. Norton and E. J. Fernandez, *AIChE J.*, **43**, 409 (1997).
13. O. Manickam and G. M. Homsy, *J. Fluid Mech.*, **288**, 75 (1995).
14. J. Azaiez and B. Singh, *Phys. Fluids*, **14**, 1557 (2002).
15. S. H. Hejazi, P. M. J. Trevelyan, J. Azaiez and A. De Wit, *J. Fluid Mech.*, **652**, 501 (2010).
16. M. Mishra, P. M. J. Trevelyan and C. Almarcha, *Phys. Rev. Lett.*, **105**, 204501 (2010).
17. Y. C. Yortsos and M. Zeybek, *Phys. Fluids*, **31**, 3511 (1988).
18. C. T. Tan and G. M. Homsy, *Phys. Fluids*, **31**, 1330 (1988).
19. F. Doumenc, T. Boeck, B. Guerrier and M. Rossi, *J. Fluid Mech.*, **648**, 521 (2010).
20. R. A. Wooding, *ZAMP*, **13**, 255 (1962).
21. Y. Ben, E. A. Demekhin and H.-C. Chang, *Phys. Fluids*, **14**, 999 (2002).
22. D. Pritchard, *Eur. J. Mech. B/Fluids*, **28**, 564 (2009).
23. S. Pramanik and M. Mishra, *Phys. Fluids*, **25**, 074104 (2013).
24. S. Pramanik and M. Mishra, *Chem. Eng. Sci.*, **110**, 144 (2014).
25. M. C. Kim and C. K. Choi, *Phys. Fluids*, **23**, 084105 (2011).
26. M. C. Kim and C. K. Choi, *Phys. Fluids*, **24**, 044102 (2012).
27. M. C. Kim, *Adv. Water Resour.*, **35**, 1 (2012).
28. M. C. Kim, *Transp. Porous Med.*, **97**, 395 (2013).
29. M. C. Kim, *Korean J. Chem. Eng.*, **35**, 364 (2018).
30. B. F. Farrell and P. J. Ioannou, *J. Atmos. Sci.*, **53**, 2041 (1996).
31. G. I. Barenblatt, Scaling, Self-Similarity and Intermediate Asymptotics, Cambridge University Press (1996).
32. W. B. Zimmerman and G. M. Homsy, *Phys. Fluids A*, **4**, 2348 (1992).
33. P. J. Schmid, *Annu. Rev. Fluid Mech.*, **39**, 129 (2007).
34. N. Tilton, D. Daniel and A. Riaz, *Phys. Fluids*, **25**, 092107 (2013).
35. J. T. H. Andres and S. S. S. Cardoso, *Chaos*, **22**, 037113 (2012).
36. D. Daniel, N. Tilton and A. Riaz, *J. Fluid Mech.*, **727**, 456 (2013).